

NANO MICRO
small

Supporting Information

for *Small*, DOI: 10.1002/smll.201101422

Interactions of Human Endothelial Cells with Gold Nanoparticles of Different Morphologies

Dorota Bartczak , Otto L. Muskens , Simone Nitti , Tilman Sanchez-Elsner ,

Timothy M. Millar , and Antonios G. Kanaras *

Supporting Info for:

Interactions of Human Endothelial Cells with Gold Nanoparticles of Different Morphologies.

Dorota Bartczak[†], O. L. Muskens[†], Simone Nitti[‡], Tilman Sanchez-Elsner[‡], Timothy M. Millar[‡] and Antonios G. Kanaras^{*†}

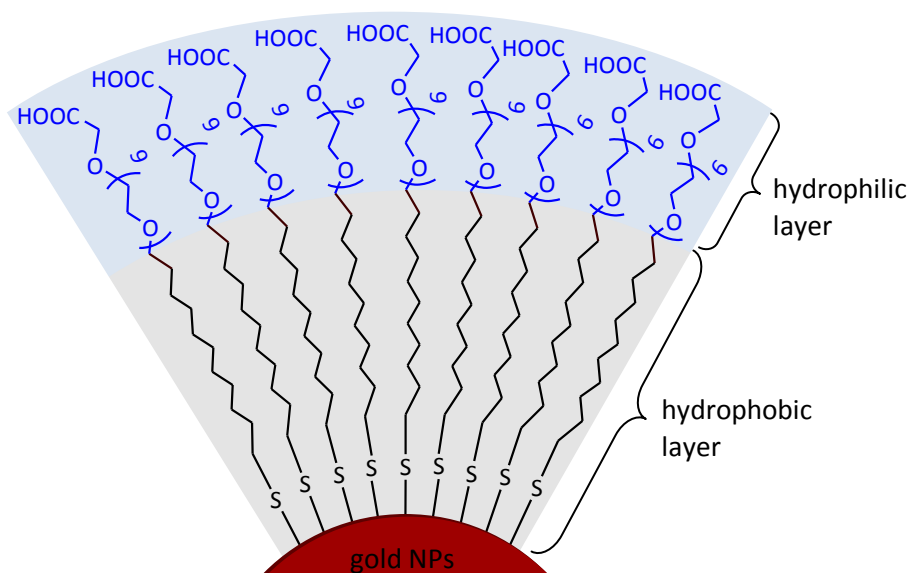
[†]School of Physics and Astronomy, [‡]School of Medicine, University of Southampton,

Southampton, SO17 1BJ, U.K. and [‡]Istituto Italiano di Tecnologia, Via Morego 30, 16163

Genova, Italy.

Sections:

- S1. Schematic representation of OEG capping layer on gold NPs.
- S2. Calculations of the number of gold atoms per nanoparticles
- S3. Quantification of OEG ligands.
- S4. Observation of OEG SP colour change, after internalisation by cells.
- S5. Statistical analysis from toxicity assay.
- S6. Calculations of laser-induced treatment
- S7. Physicochemical characterization of nanoparticles.
- S8. TEM images of cross-sectioned cells loaded with particles
- S9. Acute cytotoxicity of gold nanoparticles in endothelial cells.



Scheme S1. Schematic representation of OEG capping layer on gold NPs.

S2. Calculations of the number of gold atoms per nanoparticles

For spherical, rod-shaped, core-shell and hollow-gold particles we calculated the mass from the average volume and the known density of bulk gold. The average volume of the nanoparticles was calculated taking into account their polydispersity in the following way. For a spherical particle, the particle diameter distribution was fitted to a Gaussian profile (as shown in Fig. S1, yielding a distribution

$$P(x) = (\pi w^2)^{-1/2} \exp\left(-\frac{(x - d_{ave})^2}{w^2}\right) \quad (1)$$

Subsequently, the volume was calculated using

$$V_{ave} = \frac{4}{3} \pi \int dx P(x) x^3 = \frac{4}{3} \pi \left(d_{ave}^3 + \frac{3}{2} \frac{w^2}{d_{ave}} \right) \quad (2)$$

This formula takes into account the fact that the average volume is not the volume corresponding to the average diameter, but is biased toward larger particles in the distribution. We find a similar formula for the nanorod, where we assumed hemispherical endcaps. For core-shell and hollow-gold, the average volumes of the total minus the core particle are calculated. The above correction yields a deviation as large as 30% in the case of the silica-gold core-shell particle, as indicated by the error bars in Table 1. We also point out that in the latter case, a larger uncertainty exists due to the incomplete filling of the gold shell which is not included in our estimate because of lack of quantitative data on shell completeness.

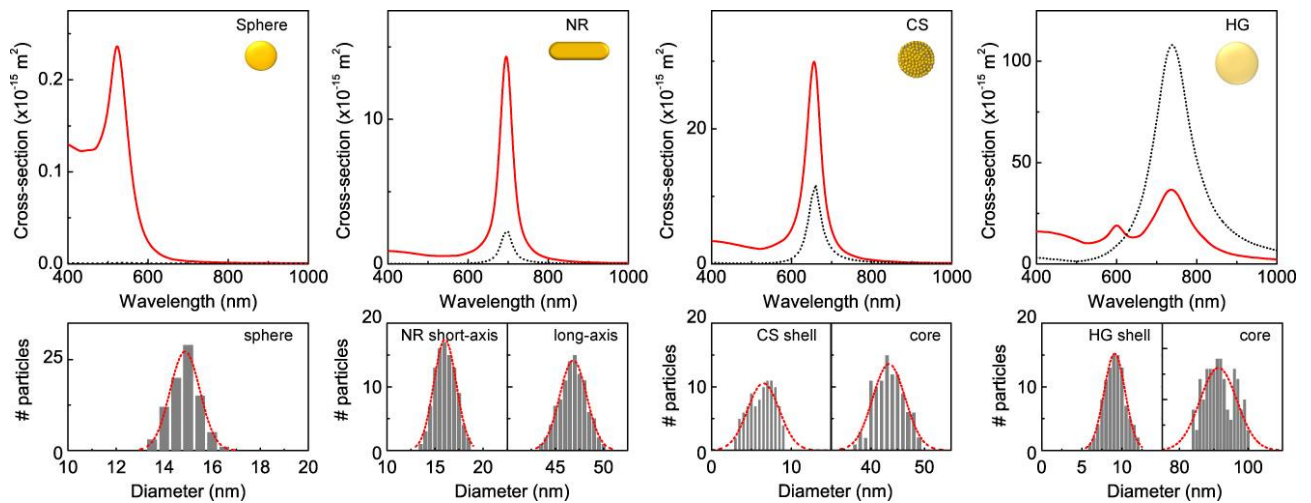


Figure S1a. Calculated absorption (red) and scattering (black) cross sections for different nanoparticle types. (Bottom) Size histograms obtained from TEM images. Dashed red lines are Gaussian distribution fits.

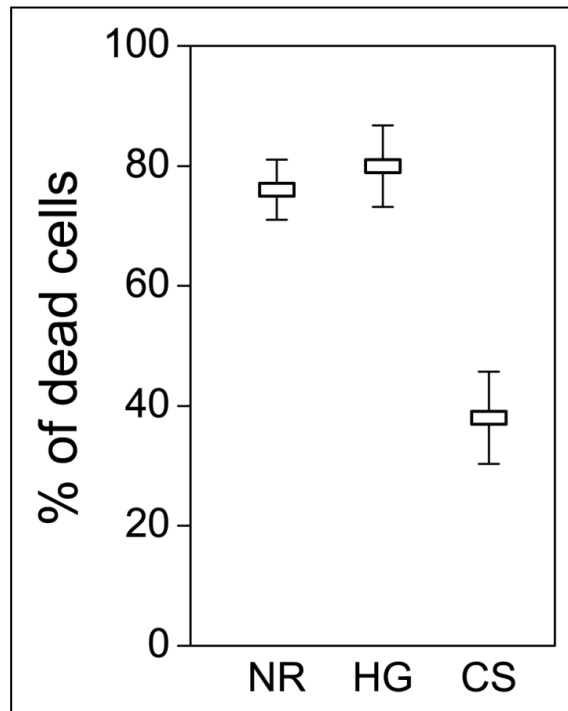


Figure S1b. Cell mortality percentages obtained when cells loaded with different types of OEG-capped NPs were treated with laser irradiation. The figure summarizes experimental results obtained in ref.14, and used here for our model.

S3. Quantification of OEG ligands.

Table S1. Estimated number of OEG ligands.

Estimated number of OEGs							
SP		NR		HG		CS	
single run	average	single run	average	single run	average	single run	average
2187	1876 ± 156	6976	6820 ± 877	55898	55871 ± 570	21893	21368 ± 830
1738		6265		54996		21772	
1879		5662		55849		21533	
1787		5902		56273		20747	
2056		7798		54925		22382	
1782		7173		55626		20177	
1687		7554		55982		21156	
1798		7816		56716		21825	
1865		7432		56032		22217	
1987		5624		56413		19976	

S4. Observation of OEG SP colour change, after internalization by cells.

The simplest method involved macroscopic observations of the cell suspension. A more advanced technique based on phase contrast and bright field microscopy of cells grown on a surface was also employed.

A digital image of HUVECs suspension after treatment with OEG SP is shown in **Fig. S2**. Prior to imaging, cells (with NPs) were washed with buffer (until the solution was colourless) to remove excess of non-internalised (or non-interacting) OEG NPs, then harvested from the culture dish and suspended in a buffered solution. Differences between untreated cells (**left**) and cells, that have uptaken NPs (**right**) are evident. Reddishness of the cell suspension, indicating the presence of stable NPs, was perceivable to the naked-eye.



Figure S2. A digital image of HUVECs suspension in 1 x PBS. Control sample (cells only, left) and cells incubated with OEG-coated SP for 4 h (right).

Table S2. Statistical analysis for acute (24h) and chronic (96h) toxicity assays.

Acute cytotoxicity (24h)

	OEG SP			OEG NR			OEG HG			OEG CS			DMSO	cont.
	1 E13	5 E12	2.5E12	1 E13	5 E12	2.5E12	1 E13	5 E12	2.5E12	1 E13	5 E12	2.5E12	[10 %]	
cord I	102.03	105.57	106.82	93.99	97.37	97.72	107.89	112.30	112.30	106.75	114.49	111.20	107.28	4.73
	89.42	112.28	105.50	99.97	83.35	108.30	116.58	110.66	106.77	110.36	104.50	122.95	110.05	10.63
	114.65	98.87	108.14	100.68	121.64	118.93	99.20	94.13	82.45	103.15	109.49	95.79	82.68	12.78
cord II	91.42	96.63	76.14	97.37	111.94	109.03	92.34	77.34	96.16	93.92	73.22	79.19	105.20	23.71
	107.20	106.77	100.53	95.95	78.14	108.85	95.22	99.57	108.67	108.04	96.38	101.91	94.77	16.64
	92.76	89.67	102.43	95.73	100.93	75.51	94.70	89.50	97.30	88.89	116.97	102.59	100.03	30.39
cord III	113.02	112.68	118.91	122.48	123.42	100.82	95.93	99.54	90.41	117.18	91.34	83.16	101.12	37.45
	126.45	118.87	112.84	119.71	101.59	91.42	83.65	85.62	74.76	98.68	119.90	108.23	91.35	35.65
	75.33	86.14	88.33	68.90	95.74	107.42	81.21	82.22	80.18	80.19	78.20	76.77	107.54	42.94
average	101.37	103.05	102.18	99.42	101.57	102.00	96.30	94.54	94.33	100.80	100.50	97.98	23.88	100.00
stdev	7.85	5.51	6.46	7.78	7.75	6.34	5.48	6.07	6.70	5.79	8.45	7.84	6.72	4.48
ttest	0.82	0.53	0.68	0.92	0.80	0.70	0.44	0.29	0.31	0.87	0.94	0.74	1.9 E-10	
	ns	ns	ns	ns	ns	ns	ns	ns	ns	ns	ns	ns	***	

Chronic Cytotoxicity (96 h)

	OEG SP			OEG NR			OEG HG			OEG CS			DMSO	cont.
	1 E13	5 E12	2.5E12	1 E13	5 E12	2.5E12	1 E13	5 E12	2.5E12	1 E13	5 E12	2.5E12	[10 %]	
cord I	101.19	104.58	106.92	117.57	89.51	93.42	102.07	106.17	99.90	102.05	100.15	112.84	22.81	104.96
	117.27	103.41	106.25	100.21	91.04	105.21	116.65	105.26	84.84	110.70	102.56	94.54	22.65	86.44
	85.10	105.75	107.60	89.52	103.50	94.95	90.26	88.05	119.04	93.41	101.35	103.69	22.48	108.59
cord II	105.74	121.61	106.75	115.84	109.76	102.91	109.23	93.59	103.52	109.91	98.49	100.82	31.24	103.72
	100.97	90.21	94.49	92.93	103.63	110.34	106.71	87.85	103.95	93.74	102.85	90.40	34.65	89.72
	107.82	102.98	105.81	90.78	88.54	87.44	94.31	129.08	86.79	88.73	103.11	119.59	35.74	106.56
cord III	100.34	104.92	116.61	105.43	87.44	100.74	109.93	117.72	113.17	108.54	107.57	98.88	58.54	92.03
	95.21	91.47	73.58	80.73	103.11	103.31	93.39	105.98	83.11	96.84	98.49	121.36	51.29	97.44
	84.86	87.98	92.61	103.12	108.81	101.21	91.09	84.68	110.15	99.71	98.57	86.52	36.77	110.53
average	99.83	101.44	101.18	99.57	98.37	99.95	101.51	102.04	100.50	100.40	101.46	103.18	35.13	100.00
stdev	5.21	5.18	6.30	6.16	4.55	3.46	4.81	7.48	6.51	3.98	1.49	6.21	6.36	4.42
ttest	0.97	0.76	0.82	0.93	0.71	0.99	0.73	0.73	0.93	0.92	0.64	0.54	1.06E-09	
	ns	ns	ns	ns	ns	ns	ns	ns	ns	ns	ns	ns	***	

p > 0.05 are treated as not significant and marked as 'ns'

0.01 > p ≤ 0.05 are presented as '*'

0.001 > p ≤ 0.01 are presented as '**'

p ≤ 0.001 are presented as '***'

S6. Calculations of laser-induced treatment

For an ultrafast laser pulse, an initial nanoparticle temperature ΔT_{GNP} is achieved within one picosecond after the pulsed excitation. The particle rapidly cools down to its surroundings on a time scale of hundreds of picoseconds. If only a single GNP would be present in the illuminated area, the train of pulses would result in an average temperature ΔT_{ave} much lower than the peak temperature. However, every cell takes up a large number of nanoparticles which all act as local photothermal convertors. For a single cell, a stationary temperature ΔT_{cell} is reached on a time scale of microseconds, where the continuous heat generation is balanced by heat flow out of the cell. In most experiments, a large area containing many cells is illuminated. The heat flux between cells then leads to an even higher temperature ΔT_{spot} which is achieved on a time scale of seconds for a submillimeter illumination spot. In the following we calculate these different temperatures on different length scales using a heat diffusion model similar to the one reported by others.¹

The absorbed energy is related to the incident laser fluence F_{in} and the particle cross-section σ_a according to $E_a = \sigma_a F_{\text{in}}$. The energy absorbed by the nanoparticle is rapidly converted from the electron gas to an equilibrium lattice temperature over a timescale of 1 ps. This timescale is fast compared to diffusion of energy out of the particle, therefore we estimate the initial temperature of the nanoparticle using the lattice heat capacity, yielding

$$\Delta T_{\text{GNP}} = \frac{\sigma_a F_{\text{in}}}{c_v^{\text{Au}} V_{\text{part}}} \quad (3)$$

with $c_v^{\text{Au}} = 2.49 \times 10^6 \text{ J m}^{-3} \text{ K}^{-1}$ the heat capacity per unit volume for gold, and V_{part} the particle volume. Equation 3 indicates the highest nonequilibrium temperature that is achieved in a single GNP following pulsed laser excitation.

After the initial pulsed excitation, heat rapidly spreads out through thermal diffusion into the surroundings of the nanoparticle, on a nanosecond time scale. In the following, we do not consider the specific shape effects associated with various types of metal particles, as these effects are very local and become irrelevant for length scales larger than a few nanometers away from the GNP. Also, on time scales long with respect to the pulse repetition time of 50ns, we can approximate the pulsed heating by an average rate.

Solving the heat diffusion equation, we consider two stationary solutions corresponding to a single nanoparticle, and a nanoparticle distribution. For a single nanoparticle, the solution of the heat diffusion equation results in the following expression

$$\Delta T_{\text{ave}}(r) = \frac{\sigma_a I}{4\pi\kappa} \frac{1}{r} \quad (4)$$

with $\kappa = 0.58 \text{ W m}^{-1} \text{ K}^{-1}$ the thermal conductivity of water, $I = F_{\text{in}} f_{\text{rep}}$ the average laser intensity, f_{rep} being the laser repetition rate. For a collection of N particles homogeneously distributed within a spherical volume with radius R, we find the following solution

$$\Delta T_{\text{sphere}}(R) = \frac{3N\sigma_a I}{8\pi\kappa} \frac{1}{R} \quad (5)$$

Equation (5) can be used to describe both the temperature $\Delta T_{\text{endosome}}$ in an endosome with closely packed nanoparticles or ΔT_{cell} in the entire cell due to an average concentration of particles.

Finally, we also consider effects of heating of a macroscopic area with many cells containing nanoparticles. Assuming a monolayer of cells, we integrate the solution of the heat

equation in this case over a two-dimensional circular area, resulting in the average temperature rise within the illumination area given by

$$\Delta T_{spot}(R) = \frac{N\sigma_a I}{2\pi\kappa} \frac{1}{R} \quad (6)$$

Table S3. Calculated temperature rise on various length scales

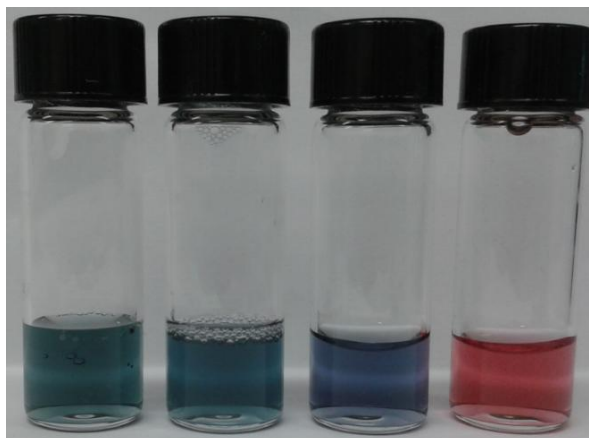
OEG NPs type	ΔT_{GNP} [°C]	ΔT_{ave} [°C]	$\Delta T_{\text{endosome}}$ [°C] (1 μm , 100 GNP)	ΔT_{cell} [°C](10 μm)	ΔT_{spot} [°C] (200 μm , 100 cells)
spherical	0.8	0.0002 \pm 0.00004	0.006 \pm 0.001	0.015 \pm 0.002	0.2 \pm 0.03
rod-like	3.2 1.0 (random)	0.006 \pm 0.0010 0.002 \pm 0.0003	0.04 \pm 0.01	0.14 \pm 0.07	1.8 \pm 0.6
hollow	0.4	0.015 \pm 0.004	0.45 \pm 0.13	0.06 \pm 0.04	0.85 \pm 0.54
core/shell	1.6	0.012 \pm 0.008	0.38 \pm 0.14	0.1 \pm 0.1	1.3 \pm 1.2

References

1. Govorov, A. O.; Richardson, H. H. NanoToday **2007**, 2, 30-38.

S7. Physicochemical characterization of nanoparticles

a) Digital images of nanoparticles' solutions.



b) UV-Visible spectra of gold nanoparticles:

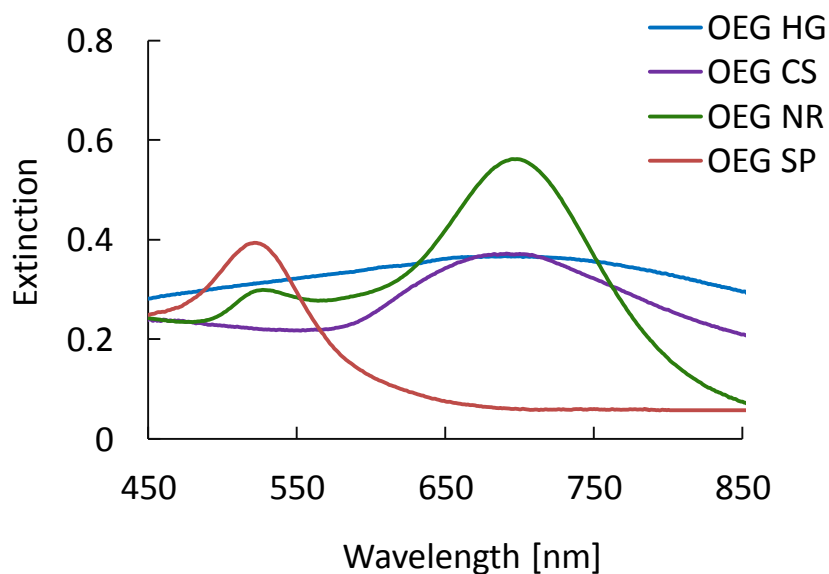


Figure S3. a) Digital images of OEG- coated nanoparticles' solutions; from the left to right: gold nanorods, hollow gold, core/shell silica/gold and spherical NPs. b) Visible spectra of the different types of particles. It is evident that no sign of aggregation is observed. As discussed in the text when the particles are sufficiently coated with the OEG ligand are stable in stringent conditions.

S8. TEM images of cross-sectioned cells loaded with particles

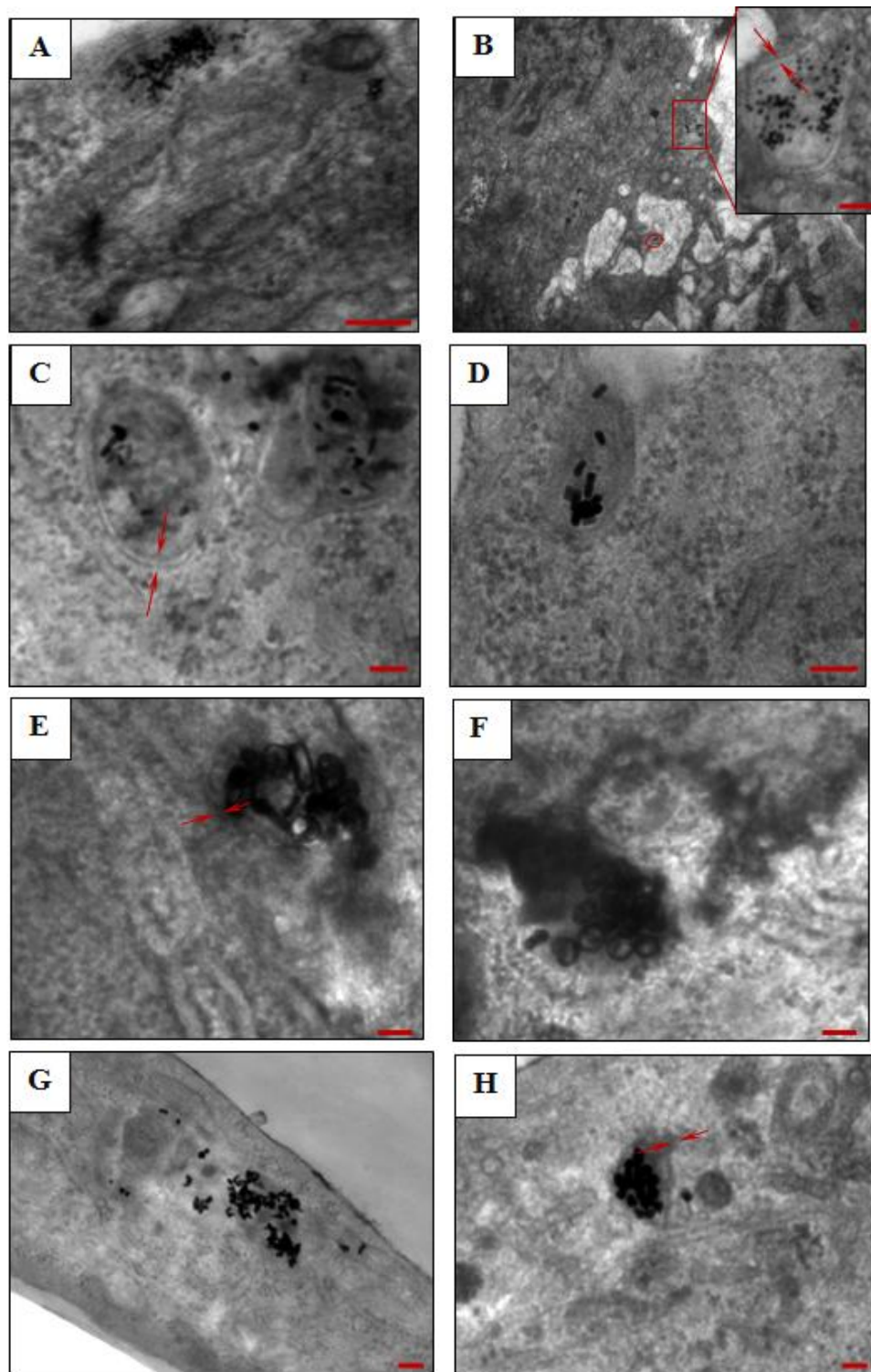


Figure S4. Lower scale TEM images in comparison to the main text. The section of the endothelial cell is better seen. After 4 h incubation with OEG SP (A, B), OEG NR(C,D), OEG

HG (E, F) and OEG CS (G, H). Double membrane is indicated by arrows. Scale bars are 100 nm.

S9. Acute cytotoxicity of gold nanoparticles in endothelial cells.

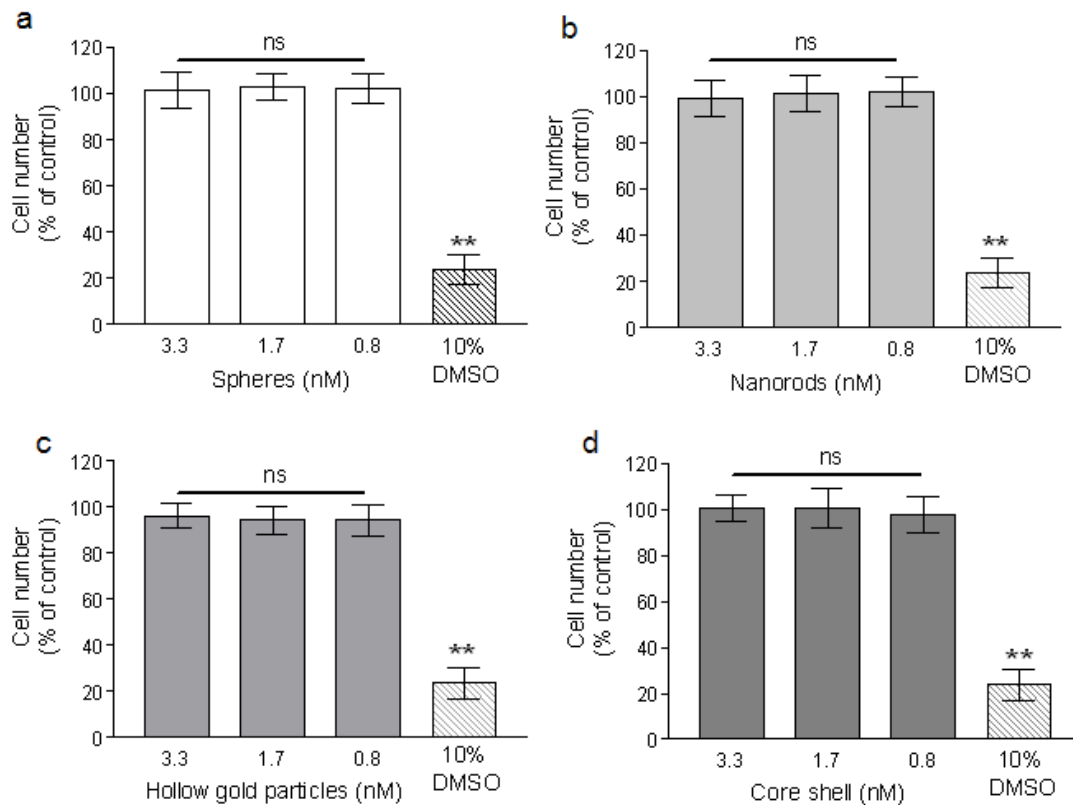


Figure S5. Acute cytotoxicity profile of endothelial cells when loaded with the different types of particles (a) spheres, (b) nanorods, (c) Hollow gold particles and (d) Core-shell silica-gold. The number of alive cells remain the same after 24 h of incubation with the particles in various concentrations. A positive control (10% DMSO) is used for comparison. t-Test analysis showing the level of significance (p) is indicated as (**) for significant and 'ns' for non-significant values (see also Table S2).